Promoting ZIF-8-Derived Fe-N-C Oxygen-Reduction Catalysts *via* Zr Doping in PEM Fuel Cells: Durability and Activity Enhancements

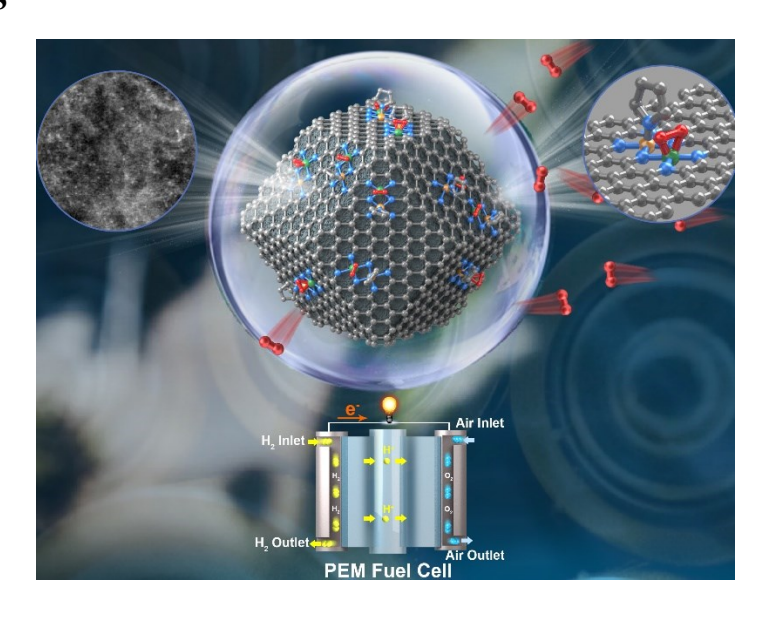
Bin Chi[#], Longhai Zhang[#], Xiaoxuan Yang, Yachao Zeng, Yijie Deng, Mingrui Liu, Junlang Huo, Chaozhong Li, Xiaorong Zhang, Xiudong Shi, Yijia Shao, Lin Gu, Lirong Zheng, Zhiming Cui, Shijun Liao*, Gang Wu*

ABSTRACT: The atomically dispersed iron site and nitrogen co-doped carbon catalysts (Fe-N-C) have demonstrated promising performance in replacing Pt towards the oxygen reduction reaction (ORR) in acids for proton exchange membrane (PEM) fuel cells. However, the insufficient durability of Fe-N-C catalysts prohibitively hinders their practical applications. Herein, we report that the co-doping of Zr and Fe single metal sites into a ZIF-8-derived mesoporous carbon exhibited significantly improved durability for the ORR. Especially, a membrane electrode assembly (MEA) from the ORR cathode catalyst only lost 25% voltage after 20 hours of continuous operation at a constant current density. After an extended test of up to 100 hours, the Zr-doped Fe-N-C catalyst retained 40% of its initial performance, superior to the catalyst without Zr doping with more than 70% activity loss after only 20 hours. The cathode also showed significantly improved ORR activity, achieving a maximum power density of 0.72 W cm⁻² under H₂/air conditions. Extensive experimental characterization and density functional theory (DFT) calculations suggested that the promoted catalytic activity and stability are due to the formation of Zr-based active sites with enhanced acidic tolerance than the individual Fe sites. Also, the doping

of Zr could suppress the formation of H_2O_2 and other free radicals, thus mitigating active site degradation. The possible Fe/Zr dual metal active sites, *i.e.*, $N_2(N)$ -Fe- N_2 -Zr- $N_2(O_2)$, likely have enhanced intrinsic ORR activity relative to conventional Fe N_x sites.

KEYWORDS: PEM fuel cells, PGM-free catalysts, single metal sites, oxygen reduction reaction, durability

TOC GRAPHICS



1. INTRODUCTION

The oxygen reduction reaction (ORR) is an essential process in the cathode of proton exchange membrane (PEM) fuel cells and determines their overall performance and durability. Due to the sluggish kinetics of the ORR in acids, current cathode catalysts are still predominantly based on Pt and its alloys. However, the scarcity and consequent high cost of Pt catalysts significantly hinder the large-scale commercialization of PEM fuel cells. Hence, an urgent need is to develop

alternative platinum group metal (PGM)-free catalysts with high catalytic activity and good durability to make PEM fuel cells affordable for large-scale transportation and other applications.²

Among the PGM-free catalyst formulations studied, transition metal single-atom doped carbon catalysts (M-N-C) are the most promising candidates due to their high activity and four-electron pathway selectivity in the challenging acidic media of PEM fuel cells.³⁻⁶ Recently, numerous M-N-C catalysts (M: Fe, Co, and Mn.⁷⁻¹²) with atomically dispersed transition metal sites have exhibited dramatically enhanced catalytic activity for the ORR in acidic aqueous electrolytes and membrane electrode assemblies (MEAs) of PEM fuel cells. In particular, single site-based Fe-N-C catalysts attracted the most attention because they have achieved promising catalytic activity and initial MEA performance.¹³⁻¹⁶

Unfortunately, current Fe-N-C catalysts doped with single Fe atoms still do not meet the requirements for practical use in H₂/air PEM fuel cells because of their unsatisfactory stability and durability. This is mainly due to the possible Fe dissolution from Fe-N_x active centers¹⁷ and corrosion of the local carbon structure, ¹⁸ likely caused by hydrogen peroxide attacks formed during cathodic oxygen reduction. ¹⁹ Thus, developing PGM-free catalysts with excellent durability and enhanced catalytic activity toward the ORR is one of the most pressing topics in this field.

During our continuous endeavors to develop highly active and durable Fe-N-C catalysts, we explore a strategy by introducing Zr to enhance catalyst stability and durability. In principle, Zr has a much better acid tolerance than Fe and can effectively suppress the production of H₂O₂ in the cathode.^{20, 21} As expected, the newly prepared Zr/Fe and N co-doped ZIF-8 derived carbon catalyst exhibited improved durability in RDE measurements and single H₂/air fuel cells.

Significantly, introducing Zr improved the durability and enhanced the catalyst activity towards ORR and the performance in a single PEM fuel cell. Although other dual transition metals codoped catalysts (such as Fe-Co,²²⁻²⁵ Fe-Ni,^{26, 27} Co-Ni,^{28, 29} and Co-Zn³⁰) have been reported previously by other groups,³¹ the atomically dispersed Zr/Fe co-doped M-N-C catalyst is the first one with earlier transition metal Zr co-doping, showing improved durability and enhanced ORR activity.

2. RESULTS AND DISCUSSION

The Fe-Zr/N/C catalyst was synthesized by pyrolyzing a Zr-doped ZIF-8 precursor at a high temperature, combined with Fe doping via a gaseous deposition method. Synthesis details were provided in the Supporting Information. An SEM image of the Zr-ZIF-8 precursor is presented in Figure 1a, showing that the Zr-ZIF-8 retained polyhedral morphology, similar to ZIF-8 crystals. XRD (Figure S1) and FT-IR (Figure S2) results confirmed that partially introducing Zr into ZIF-8 did not affect the morphology and structure (the mole ratio of Zn to Zr was 50:3). However, the Zr-ZIF-8 particle sizes were about 650 nm in diameter, much larger than ZIF-8s without Zr doping (380 nm) (Figure S3), likely due to Zr having a larger ion radius than Zn. After the Zr-ZIF-8 precursor was pyrolyzed at high temperatures, the prepared Fe-Zr/N/C (Figures 1b, c) catalyst maintained the polyhedral morphology much better than the N/C and the Fe/N/C catalysts (Figure S4), indicating the Zr-ZIF-8 particles was not easily decomposed during the pyrolysis.

Figure 1d shows a high-angle annular dark-field scanning transmission electron microscopy (HAAD-STEM) image of the Fe-Zr/N/C catalyst, revealing a porous structure with numerous bright dots. Hence, most of the Fe and Zr are dispersed atomically in the catalyst skeleton without clusters or metal particles. Figure 1e presents elemental mapping for the Fe-Zr/N/C catalyst,

showing that all four elements are uniformly distributed. Furthermore, HR-TEM images (Figure S5) and XRD patterns (Figure S8) of the Fe-Zr/N/C catalyst also confirmed that no Fe or Zr particles or aggregates existed in bulk or at the surface of the Fe-Zr/N/C catalyst.

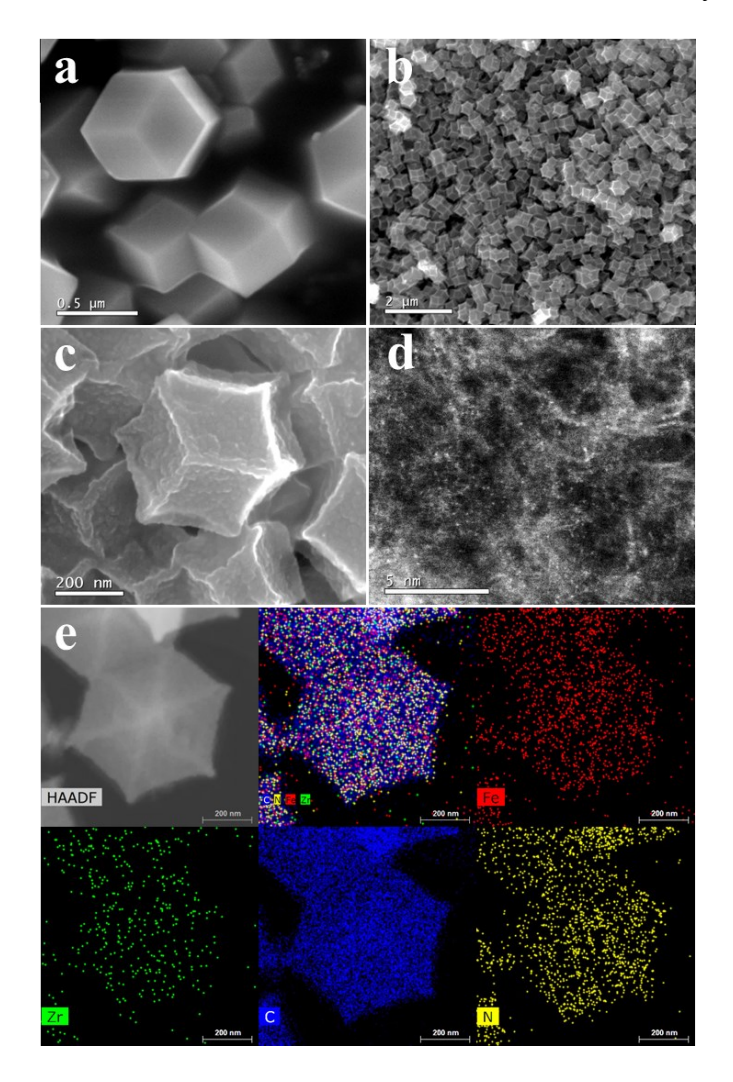


Figure 1. (a) SEM of Zr@ZIF-8 precursor; (b, c) SEM of the Fe-Zr/N/C catalyst, image (c) being an enlargement of image (b); (d) HAADF-STEM images of the Fe-Zr/N/C; (e) elemental mapping of the Fe-Zr/N/C catalyst.

Figure S8a compared XRD patterns of the Fe-Zr/N/C, the Fe/N/C, the Zr/N/C, and the N/C. Only carbon diffraction peaks can be observed for all samples, indicating that Fe and Zr were

atomically dispersed in the catalyst skeleton after pyrolysis during preparation. The Raman spectra present that the I_D/I_G ratios for the N/C, the Zr/N/C, the Fe/N/C, and the Fe-Zr/N/C are 1.02, 1.01, 1.04, and 1.10, respectively (Figure S8b). The highest ratio for the Fe-Zr/N/C indicated the most abundant defect sites in the Zr/Fe co-doped catalyst. Figures S8c and S8d showed that the specific surface areas of the Fe-Zr/N/C and the Fe/N/C catalysts were 1086.5 and 935.3 m²/g, respectively. The Fe-Zr/N/C catalyst had a 10% higher specific surface area due to its higher porosity and a more significant number of defect sites, which could be beneficial for exposing more active sites.

Figures 2a and b show the Fe 2p and N 1s spectra of the Fe-Zr/N/C and the Fe/N/C catalysts, respectively. The electronic structures of Fe and N were influenced by introducing Zr into the catalyst. Compared with the Fe/N/C catalyst, the binding energy of the N and Fe species in the Fe-Zr/N/C shifted positively by 0.2 and 0.3 eV, respectively. In addition, the deconvolution results of the N 1s spectrum of the Fe-Zr/N/C catalyst present a new peak at 397.4 eV, likely related to the doped Zr sites. Thus, we speculated that Zr-N_x moieties also existed in the Fe-Zr/N/C catalyst in addition to traditional FeN_x sites. Figure 2c presents the Zr 3d spectra of the Fe-Zr/N/C and the Zr/N/C catalysts. The binding energy of the Zr in the Fe-Zr/N/C shifted negatively by 0.6 eV compared to the Zr/N/C, suggesting substantial electron transfer to the Zr sites due to the coexistence of Fe or strong interactions between Zr and N ligands. On the contrary, the binding energies of Fe and N species in the catalyst were shifted positively (see Figures 2a and b), and the distribution of various N dopants was changed significantly. Thus, the Zr-N_x moieties likely coexisted with Fe-based active sites in the catalyst through an N bridge (see Figure 2d). These Zrbased active sites probably have better activity than the Fe-based ones because more electron was

transferred to Zr sites capable of weakening the adsorption of O₂ and intermediates on Fe sites.³² Therefore, the formation of Zr-based active sites (Zr-N moieties) and the significant change in the N structure distribution are critical factors to the enhanced ORR activity and durability.^{33, 34} Furthermore, the N content in the Fe-Zr/N/C was higher than the Fe/N/C (4.55% and 0.55%, shown in Table S1), which facilitates the formation of nitrogen-coordinated single metal active sites.

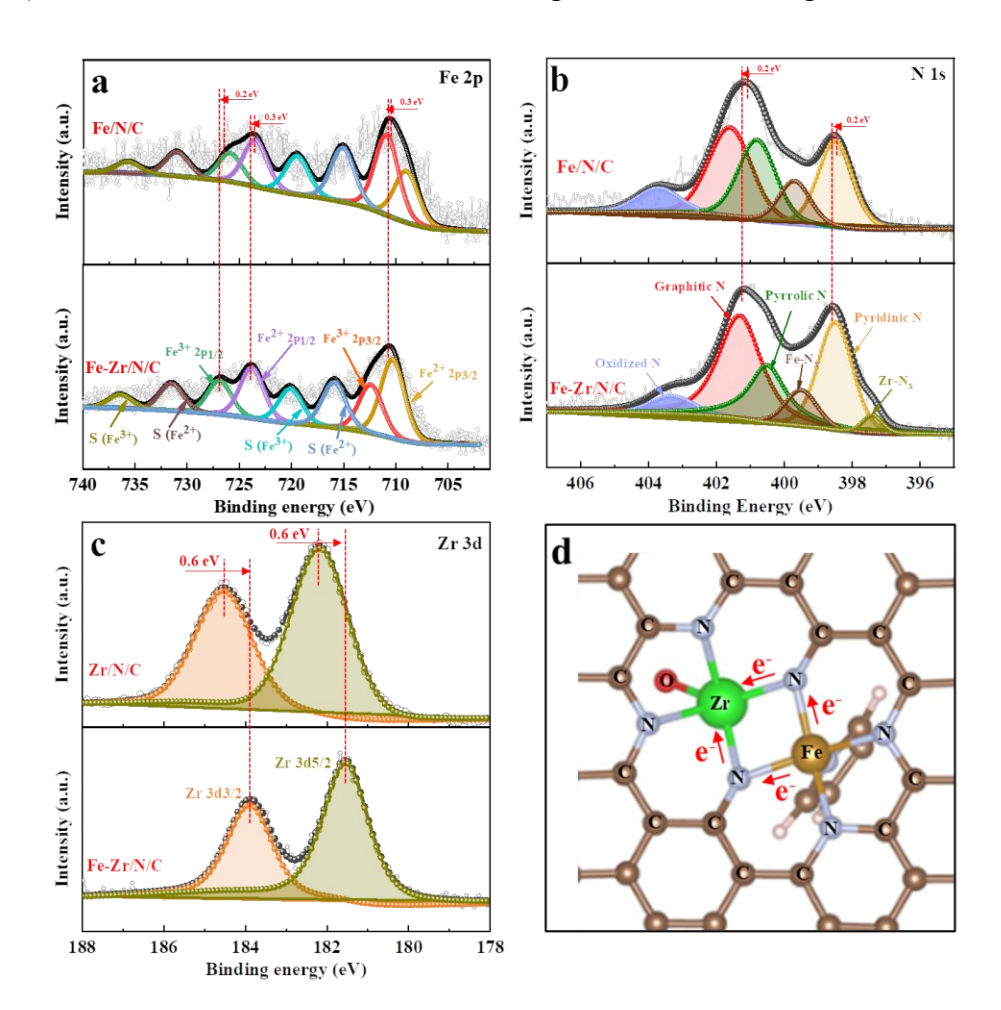


Figure 2. High-resolution N 1s (a) and Fe 2p (b) XPS spectra of Fe-Zr/N/C and Fe/N/C; (c) high-resolution Zr 3d XPS spectra of Fe-Zr/N/C; (d) schematic diagram of the dual active sites in the Fe-Zr/N/C catalyst and the charge transfer situation (details of active site structure configuration showing at Figure 5a).

To understand the promotion role of Zr doping, ⁵⁷Fe Mössbauer spectral analysis was conducted. As shown in Figure 3a, only three doublets were deconvoluted, using the isomer shift (IS) and quadrupole splitting (QS) values: D1, D2, and D3. Among these, D1, with the largest IS value of 0.33 and a QS value of 1.09, was assigned to the intermediate-spin species Fe^{III}N₄. ³⁵ D2 was assigned to the low-spin species Fe^{II}N₄, which had an IS value of 0.26 and a QS value of 2.61. D3, with an IS value of 0.13 and the largest QS value of 0.42, was assigned to the high-spin species N-(Fe^{III}N₄), ^{35, 36} indicating that Fe-N₅ moieties existed as one of the main Fe-N structures in the Zr-Fe/N/C catalyst.

X-ray absorption near-edge structure (XANES), extended X-ray absorption fine structure (EXAFS), and wavelet transform (WT) were further conducted to reveal changes in the chemical state and coordination environment of Fe and Zr sites. The XANES spectra of the Fe K-edge absorption (Figure 3b) show that the Fe K-edge energy absorption threshold values of the Fe/N/C and the Fe-Zr/N/C located between the reference Fe foil and Fe₂O₃,³⁷ indicating the chemical state of Fe in both catalysts is between Fe⁰ and Fe³⁺, but more closer to Fe³⁺. Figure 3d presents the Fourier transform (FT) k³-weighted χ (k)-function curves (R space) of the Fe K-edge EXAFS spectra. The prominent peak for the Fe/N/C and the Fe-Zr/N/C is around 1.40 Å, which is assigned to the dominant Fe-N(O) coordination,^{37, 38} without Fe-Fe peaks observed in either spectrum. Therefore, Fe species in both catalysts existed as atomic sites likely coordinated with N(O).

EXAFS wavelet transform was the most effective way to analyze the backscattering of atoms in the catalysts. The WT of Fe-Zr/N/C presented in Figure 3f indicates an intensity maximum at 5 $Å^{-1}$ in the *k*-space, which was very close to that of FePc (~4.8 Å⁻¹) but far different from the values

for Fe foil (\sim 8 Å⁻¹) and Fe₂O₃ (\sim 8.2 Å⁻¹) (as displayed in Figure S13), confirming Fe existed primarily as FeN_x moieties. Similarly, the Zr K-edge energy absorption threshold value of the FeZr/N/C catalyst was higher than that of the reference Zr foil and closer to that of ZrO₂ (Figure 3c), confirming that the chemical state of Zr was closer to Zr⁴⁺. Further, the central peak of Zr K-edge EXAFS occurred 1.50 Å from the Zr R space (Figure 3e), which was assigned to Zr-N(O) coordination. In contrast, no peaks for Zr-Zr (2.91 Å) were present, indicating that Zr either was coordinated only with N(O) or was atomically dispersed in the sample. The WT of the Fe-Zr/N/C showed an intensity maximum at 5 Å⁻¹ in the *k*-space, compared with 9.5 Å⁻¹ for the Zr foil (Figure S14), further confirming the atomic dispersion of Zr species in the catalyst. Thus, combined with the results of XAS analysis, we can conclude that Fe and Zr are atomically dispersed within the catalyst, primarily coordinated with N or O atoms.

The EXAFS fitting results of the Fe-Zr/N/C catalyst elucidated the coordination environments of Fe and Zr sites (Figures S15a and b). The average coordination number of Fe-N (Table S4) was 5.0 rather than the usual 4.0, indicating that Fe-N(O) coordination in the Fe-Zr/N/C catalyst was mainly in the form of Fe-N(O)s, which was likely more active than Fe-N₄. The WT analysis results further supported the formation of new moieties. The intensity maximum of the Fe-Zr/N/C was shifted slightly compared with the Fe/N/C, dominated by Fe-N₅ moieties. Meanwhile, the Zr-N(O) coordination environment in the Fe-Zr/N/C was mainly Zr-N(O)6, as the average coordination number was approximately 6.1 (Table S5). In comparison, the coordination environment of Fe-N(O) in the Fe/N/C catalyst was mainly Fe-N(O)4, according to the EXAFS fitting results (Figure S16 and Table S4). These fitting results confirmed that Fe and Zr were dispersed in the catalyst as single metal sites, as the central coordination structures of Fe-N₅ and

ZrN₆, respectively. The Fe-N₅ moiety in the Fe-Zr/N/C has a lower reaction energy barrier and lower absorption energy of intermediate OH than the usual Fe-N₄ sites, contributing to higher activity and durability of catalysts. ⁴¹⁻⁴³ ZrN₆ should also contribute significantly to the enhanced stability of the catalyst. Notably, no Zr-Fe bond could be found in the EXAFS results (Figure 3). Combining the XRD and XPS results, we suggest that, similar to Fe, the Zr atoms were also atomically dispersed/doped in the catalyst, likely in the form of Zr-N moieties. Also, the atomically dispersed Fe-N and Zr-N moieties likely are connected through N bridges (shared N atoms).

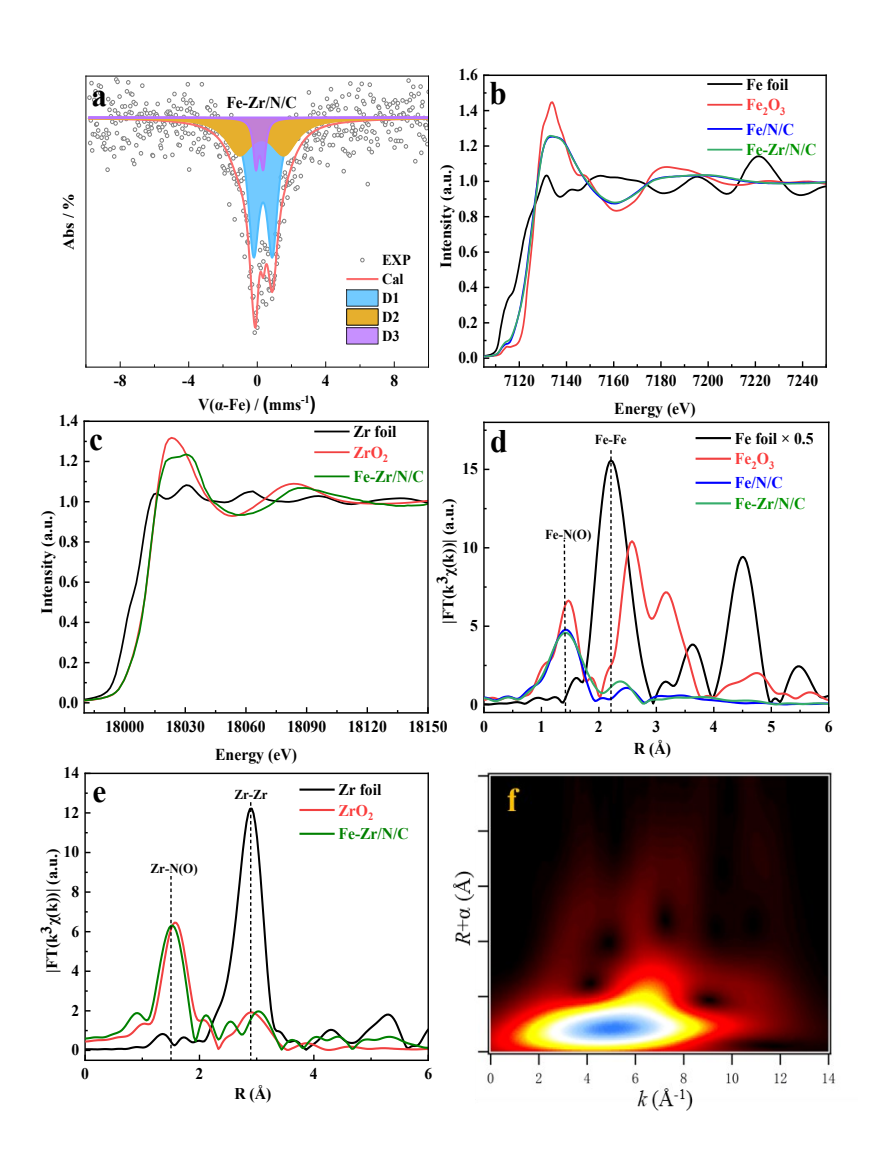


Figure 3. (a)⁵⁷Fe Mössbauer spectra of Fe-Zr/N/C; Fe K-edge XANES spectra (b) and Fourier transform of Fe K-edge EXAFS spectra (d) for Fe/N/C, Fe-Zr/N/C, and reference Fe foil, Fe₂O₃; Zr K-edge XANES spectra (c) and Fourier transform of Zr K-edge EXAFS spectra (e) for Fe-Zr/N/C and reference Zr foil, ZrO₄; wavelet transform of the k³-weighted EXAFS data for Fe/N/C and Fe-Zr/N/C (f).

Figure 4a compared the ORR activities of different samples, including the N/C, the Zr/N/C, the Fe/N/C, and the Fe-Zr/N/C, in O₂-saturated 0.1 M HClO₄. The Fe-Zr/N/C catalyst achieved a half-wave potential of up to 0.872 V (vs. RHE), 52 mV higher than the Fe/N/C catalyst (0.820 V vs. RHE) and only 11 mV less than a commercial Pt/C catalyst (60 μg_{Pt}cm⁻²). As shown in Figure 4c, the kinetic current density of the Fe-Zr/N/C catalyst at 0.8 V (vs. RHE) was 5.6 times higher than that of the Fe/N/C, revealing the promotional role of Zr co-doping in activity enhancement. We calculated the electrochemically active surface area (ECSA; see Figure S17) of the catalysts by estimating it from the double-layer capacitance (C_{dl})⁴⁴ to compare the intrinsic activity of the studied catalysts. The Fe-Zr/N/C catalyst possessed a 2.5-times higher ECSA than the Fe/N/C. This was consistent with the specific surface area results, implying that the improved performance of the Fe-Zr/N/C is partially due to the larger surface area induced by Zr co-doping and the enhanced intrinsic activity.

We also used a rotating ring-disk electrode (RRDE) to analyze the electron transfer number and H₂O₂ yield of the studied catalysts. In Figure S19 and Figure 4b, the electron transfer number of the Fe-Zr/N/C catalyst was much closer to four electrons than that of the N/C, the Zr/N/C, and the Fe/N/C. In addition, the H₂O₂ yield of the Fe-Zr/N/C at 0.5 V vs. RHE was 1.09% (Figure 4d),

which was similar to a Pt/C catalyst and far less than that of the N/C (17.59%), the Zr/N/C (13.19%), and the Fe/N/C catalyst (7.51%), indicating the strong inhibitory effect of Zr towards the formation of H_2O_2 during the ORR. This conclusion was also supported by the H_2O_2 yield data measured with various catalyst loadings in an electrode disk, as shown in Figure S20. There are few previous reports of such a low H_2O_2 yield, likely due to Zr co-doping, resulting in better catalyst selectivity towards four-electron reduction and enhanced durability because H_2O_2 formation was effectively suppressed.

Further, the nitrite (NO₂⁻) poisoning and electrochemical stripping method developed by Kucernak et al. 45 was adopted to measure the site density (SD) of the Fe/N/C and the Fe-Zr/N/C catalysts. The nitrite stripping measurements were performed in an acetate buffer electrolyte (pH 5.2). Well-defined nitrite stripping peaks were observed for the poisoned catalysts between - 0.3~0.2 V vs. RHE. The Fe/N/C and Fe-Zr/N/C catalysts achieved the stripping charge of 21.55 and 46.48 C g⁻¹, shown in Figure S34. The SD values of the Fe/N/C and the Fe-Zr/N/C catalysts were 5.08×10^{20} and 1.10×10^{21} sites g⁻¹, respectively, calculated using the stripping charge (calculation equations shown in the Supporting Information). The higher SD values of the Fe-Zr/N/C catalyst also explained its improved catalytic activity than the Fe/N/C, indicating that the co-doping of Fe and Zr single atoms in the catalyst significantly increased the density of active sites.

A series of MEAs were prepared with the studied catalysts as the cathode, including the Fe/N/C, the Fe-Zr/N/C, and a commercial Pt/C, and measured under hydrogen/air (or oxygen) single PEM fuel cells. As shown in Figures 4e and f, the MEA with the Fe-Zr/N/C cathode achieved

outstanding performance, comparable to a Pt/C cathode (0.1 mg_{Pt}cm⁻²) in a low current density range, verifying that co-doping with Zr sites boosted the catalytic activity of the Fe/N/C. Under H₂/O₂ at a pressure of 200 kPa, the MEA with the Fe-Zr/N/C cathode (loading of 2 mg cm⁻²) generated current densities of 1.0 and 1.75 A cm⁻² at 0.7 and 0.6 V, respectively. The maximum power density reached 1.20 W cm⁻², significantly higher than the Fe/N/C catalyst (0.55 and 1 A cm⁻² at 0.7 and 0.6 V, and the maximum power density 0.76 W cm⁻² under identical conditions). Under practical 200 kPa H₂/air conditions, the MEA generated current densities of 0.7 and 1.1 A cm⁻² at 0.7 and 0.6 V, respectively, and the maximum power density reached 0.72 W cm⁻², higher than the Fe/N/C cathode and only slightly lower than the typical Pt/C cathode. In Figure 4g, the MEA with the Fe-Zr/N/C cathode achieved a current density up to 0.04 A cm⁻² at 0.9 V_{iR-free} under H₂/O₂ at a pressure of 150 kPa, close to the U.S. Department of Energy's 2025 target (0.044 A cm⁻² at 0.9 V_{iR-free}).

To better understand the promotional role of Zr co-doping, electrochemical impedance spectroscopy (EIS) was conducted on MEAs with the Fe-Zr/N/C and the Fe/N/C cathodes. As shown in Figure S22, they had almost the same ohmic impedance (0.0324 Ω cm² for the Fe-Zr/N/C and 0.0325 Ω cm² for the Fe/N/C), a characteristic mainly determined by membrane resistance. However, the MEA with the Fe-Zr/N/C cathode had a much lower charge transfer resistance (0.0147 Ω cm²) than the Fe/N/C cathode (0.0258 Ω cm²), indicating the Fe-Zr/N/C possessed improved catalytic activity due to the formation of Zr-based active sites, which is consistent with the RDE and MEA performance results.

We also investigated the effect of the Fe-Zr/N/C cathode loadings on MEA performance

(Figure S24). The MEA presented good performance with a low loading in both H₂/O₂ and H₂/air single PEM fuel cells. Notably, when the loading was only 1 mg cm⁻², the maximum power density decreased by just 5% compared with a catalyst loading of 2 mg cm⁻². We thus speculated that the Zr co-doping endowed a richly porous structure of the Fe-Zr/N/C catalyst due to larger polyhedron sizes, more well-defined morphology, and higher surface areas. Also, the Zr co-doping led to a new active site moiety associated with Zr sites, which enhanced the catalyst activity.

Significantly, the Fe-Zr/N/C catalyst exhibited superior activity and improved durability. According to the chronoamperometry results (Figure S21) measured at 0.62 V (vs. RHE) in 0.1 M HClO₄ solution, the current retention of the Fe-Zr/N/C catalyst was 95.44% after 48,000 s higher than 83.36% for the Fe/N/C catalyst. The enhanced durability of the Fe-Zr/N/C catalyst was also observed in an actual single PEM fuel cell. When the cell was fed with hydrogen and pure oxygen (Figure S25), the voltage of the MEA with the Fe-Zr/N/C cathode decayed only 25.3% after 20 hours at a constant current density (1.0 mA/cm²), compared with a decay of 72.4% of the Fe/N/C catalyst cathode under identical conditions. After 100 hours of continuous operating, it retains 40% of its initial voltage (Figure 4h). The output power density of the Fe-Zr/N/C cathode was 509 mW cm⁻², which was higher than the Fe/N/C (178 mW cm⁻²) after 20 hours of operation. Continuous operating for up to 100 hours, the output power density of the Fe-Zr/N/C cathode was also maintained at 277 mW cm⁻², indicating a more stable output performance. We ascribe the improved durability to two factors. One is the superior acid tolerance of Zr compared to Fe, which means that Zr-based active sites remain more stable in an acidic environment. The second is the inhibition of H₂O₂ formation in the presence of Zr. This was confirmed by the RRDE analyses, which the H₂O₂ yield for the Fe-Zr/N/C sample was much lower than that of the Fe/N/C catalyst (see Figures 4b and d).

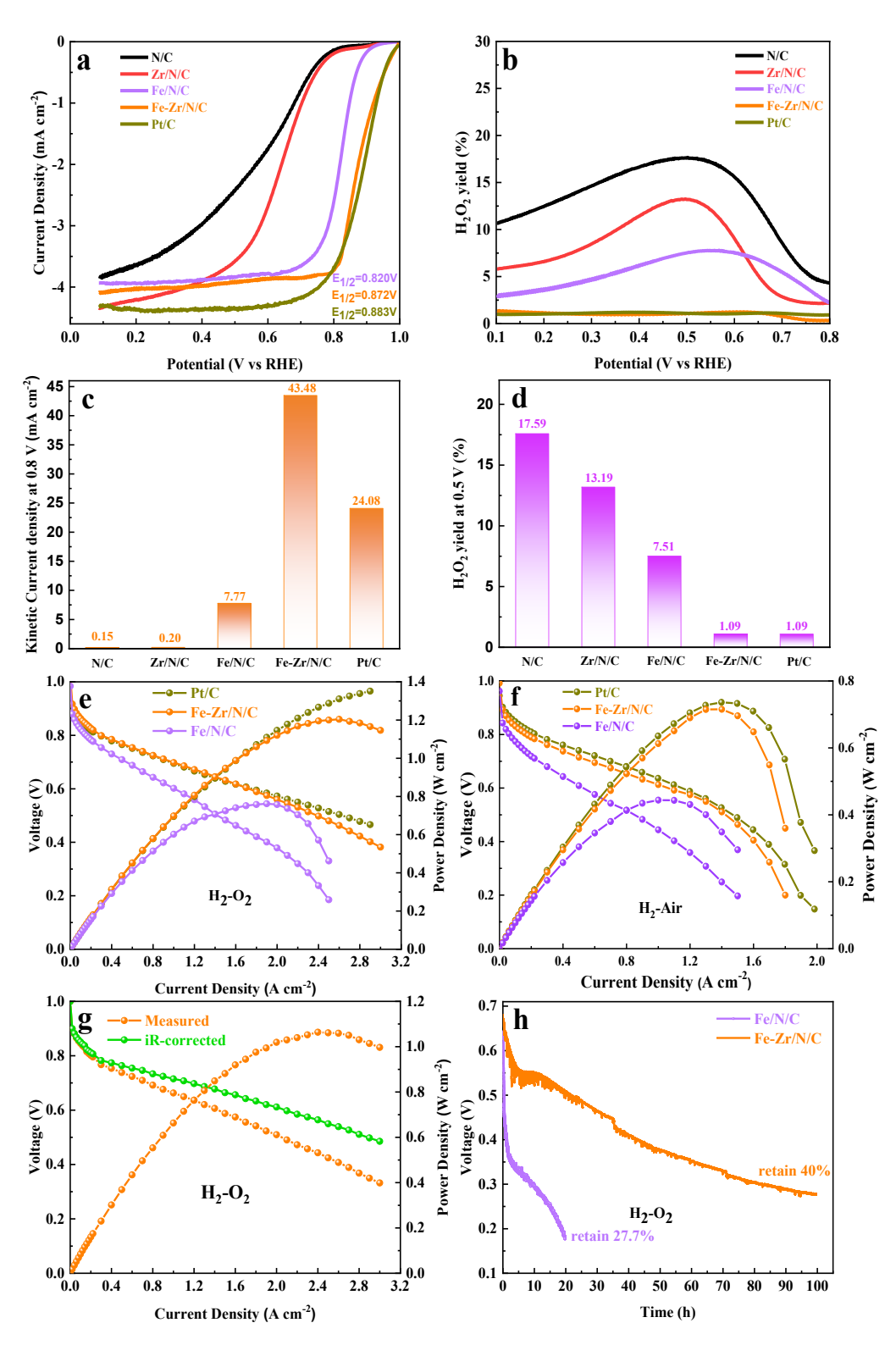


Figure 4. (a) LSV curves, (b) H₂O₂ yield, (c) Kinetic current density at 0.8 V and (d) H₂O₂ yield at 0.5 V of N/C, Zr/N/C, Fe/N/C, Fe-Zr/N/C, and Pt/C (60 μg Pt on the electrode disk) in O₂-saturated 0.1 M HClO₄ with a rotation speed of 900 rpm and a catalyst loading of 0.8 mg cm⁻²; Single PEM fuel cell performance of Fe-Zr/N/C, Fe/N/C, or Pt/C (cathode Pt loading was 0.2 mg cm⁻²) as cathode catalyst in conditions of 200 kPa H₂/O₂ (e) and H₂/air (f); (g) Fuel cell performance of Fe-Zr/N/C fed with 150 kPa H₂/O₂; (h) Voltage retention of Fe-Zr/N/C or Fe/N/C as the cathode catalyst after long-time discharge, fed with H₂/O₂ at a constant current density of 1 A cm⁻². A single PEM fuel cell was operated at 80°C and 100% RH, and the loading of Fe-Zr/N/C and Fe/N/C in the cathode catalyst layer was 2 mg cm⁻², while the Pt loading in the anode catalyst layer was 0.1 mg cm⁻²; the membrane was Nafion® 211, and the mass ratio of Nafion to Fe-Zr/N/C catalyst in the cathode catalyst layer was 1:2.

DFT calculations were conducted further to understand the intrinsic catalytic activity of the catalyst due to Zr doping. Based on the extensive experimental characterization, we propose a new dual-active-site structure (key active sites in catalyst), N₂(N)-Fe-N₂-Zr-N₂(O₂), for the Fe-Zr/N/C catalyst, wherein Fe and Zr are correlated through N bridges, and oxygen may take part in the structure of Zr-based active sites, as shown in Figures S26 and S27. The axial pyrrolic-N is the fifth N coordinated with the Fe sites and Zr is coordinated with four N in a plane and two O in the axial, as shown in Figure 5a.

Figure 5b and Figure S28 show the optimized adsorption structure of all intermediates, including *O₂, *OOH, *O, and *OH, adsorbed on the active sites of N₂(N)-Fe-N₂-Zr-N₂(O₂) and Fe-N₄, as well as the ORR evolution program. To gain insight into the catalytic activity of the

N₂(N)-Fe-N₂-Zr-N₂(O₂) active sites, the change in Gibbs free energy for every ORR elementary reaction was calculated (Table S6). Figure 5c presents the results for the N₂(N)-Fe-N₂-Zr-N₂(O₂) and a Fe-N₄ site graphically, showing the rate-determining step of the Fe-Zr/N/C and the Fe/N/C was *O₂ hydrogenation to *OOH. The energy barrier of the N₂(N)-Fe-N₂-Zr-N₂(O₂) site for this step was 0.56 eV with an applied potential of 1.23 V, which was much lower than that of a FeN₄ site (0.71 eV), suggesting the N₂(N)-Fe-N₂-Zr-N₂(O₂) site could be kinetically favorable for reducing O₂ to H₂O. The *d*-band center of the N₂(N)-Fe-N₂-Zr-N₂(O₂) and Fe-N₄ sites were further analyzed to explain the enhanced catalytic activity. As displayed in Figure S32, the d-band center of the N₂(N)-Fe-N₂-Zr-N₂(O₂) site was -1.19 eV, a negative shift compared to Fe-N₄ (-1.16 eV). The downshift of the *d*-band center could weaken the absorption of oxygen molecules/intermediates, enhancing intrinsic ORR activity.

DFT calculations also elucidate the enhanced stability observed with the Fe-Zr/N/C catalyst (Figure 5d). The formation energy of the N₂(N)-Fe-N₂-Zr-N₂(O₂) site was -12.99 eV, more negative than a FeN₄ site (-2.50 eV), suggesting enhanced thermodynamic stability against chemical dementallation.⁷ Figures 5e and f display the charge density and Bader charge distribution in the N₂(N)-Fe-N₂-Zr-N₂(O₂) site, respectively. Compared with a FeN₄ site (Figure S33), significant electrons (about 0.04 e) in the N₂(N)-Fe-N₂-Zr-N₂(O₂) site transfer from Fe to N, resulting in weaker adsorption of O₂, consistent with the XPS results.

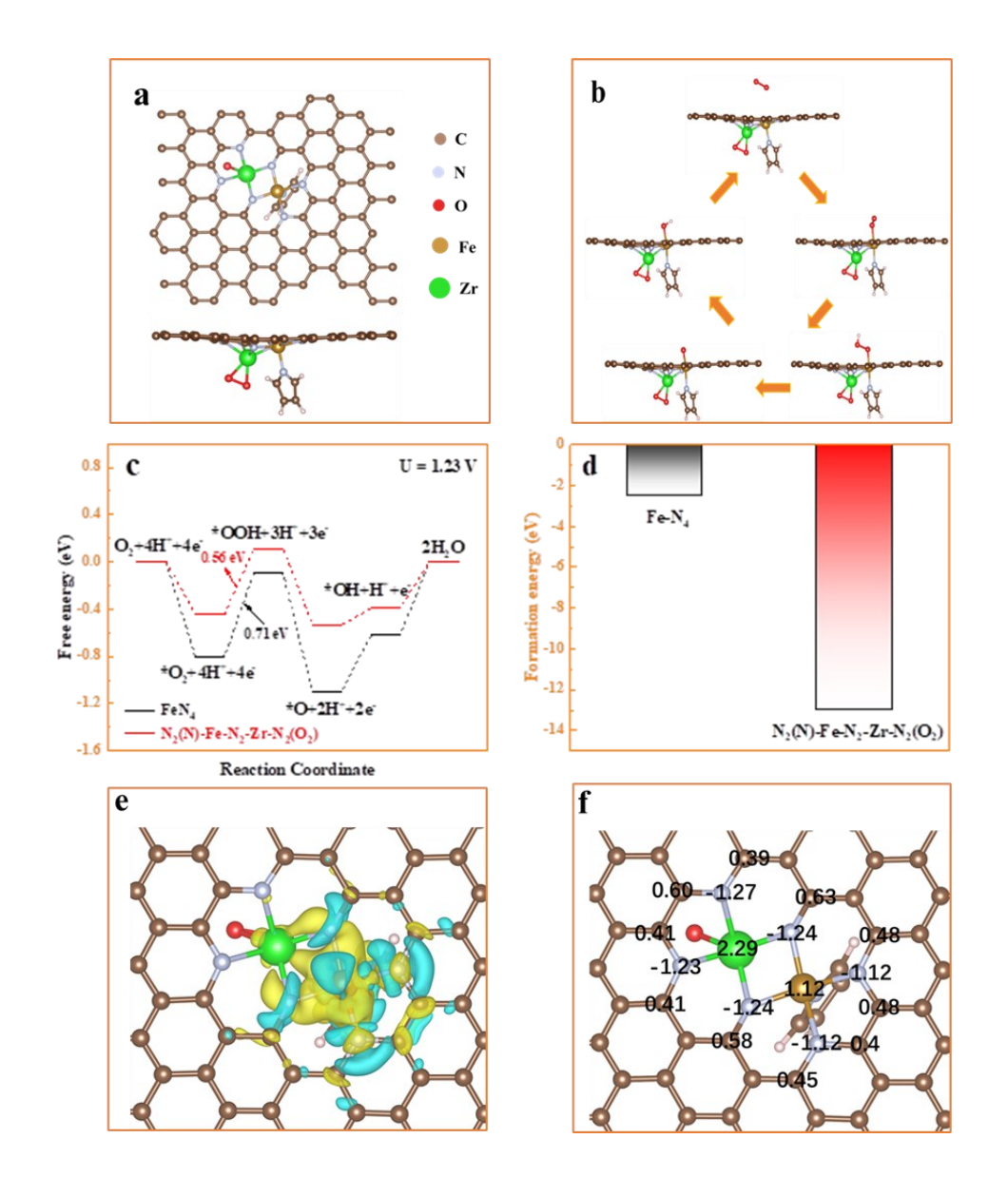


Figure 5. (a) Optimized structure of N₂(N)-Fe-N₂-Zr-N₂(O₂); (b) optimized structures of *O₂, *OOH, *O, and *OH absorbed on N₂(N)-Fe-N₂-Zr-N₂(O₂); (c) free energy diagram of the reduction of O₂ to H₂O on N₂(N)-Fe-N₂-Zr-N₂(O₂) and Fe-N₄; (e) the charge density and (f) Bader charge distribution in N₂(N)-Fe-N₂-Zr-N₂(O₂), with the yellow area representing charge density increase and the light blue area representing charge density decrease.

3. CONCLUSIONS

In summary, we report a highly active and durable carbon catalyst co-doped with atomic Zr and Fe (Fe-Zr/N/C), with a well-defined polyhedron morphology and atomically dispersed Zr and Fe. The dual metal site catalyst was prepared by a pyrolysis process using Zr-doped ZIF-8 as the Zr precursor and ferrocene as the gaseous Fe precursor. The introduction of atomic Zr significantly improved the catalyst stability, especially in actual hydrogen/air single PEM fuel cells. The stability enhancement can be ascribed to forming Zr-based active centers (Zr-N_x moieties) with much-enhanced acid tolerance than Fe-N_x moieties. Also, the Zr site doping suppressed the generation of H₂O₂, which mitigates carbon and active site oxidation. The possible synergy between Zr and Fe could make Fe sites more acid tolerant. The introduction of the atomic Zr sites also greatly enhanced the ORR intrinsic activity due to the formation of a new dual-metal site, likely in the form of N₂(N)-Fe-N₂-Zr-N₂(O₂). The newly achieved MEA performance represents one of the best-reported PGM-free catalysts for PEM fuel cells. This study demonstrated an effective strategy for a carbon catalyst doped with two atomic-scale transition metals (late transition metal Fe and early transition metal Zr) that exhibited improved performance and durability in an actual PEM fuel cell. The approach may further provide a solution to design dual metal site catalysts for other critical electrocatalysis processes such as oxygen reduction to H₂O₂, ⁴⁷ CO₂ reduction reaction⁴⁸ and nitrogen electrochemical reactions.^{49, 50}

ASSOCIATED CONTENT

The Supporting Information is available free of charge at https://pubs.acs.org/doi/10.1021/xxx.

additional SEM, TEM, XRD, BET, Raman, and electrochemical tests for the studied catalysts and comparison samples; relevant theoretical modeling and DFT calculations to study improved ORR activity and stability; curve fitting parameters for Fe and Zr K-edge EXAFS; and fuel cell MEA performance and durability (PDF)

AUTHOR INFORMATION

Corresponding Authors

Shijun Liao - The Key Laboratory of Fuel Cell Technology of Guangdong Province & the Key Laboratory of New Energy Technology of Guangdong Universities, School of Chemistry and Chemical Engineering, South China University of Technology, Guangzhou, Guangdong 510641, China; E-mail: chsjliao@scut.edu.cn

Gang Wu - Department of Chemical and Biological Engineering, University at Buffalo, The State University of New York, Buffalo, New York 14260, USA; E-mail: gangwu@buffalo.edu

Authors

Bin Chi - The Key Laboratory of Fuel Cell Technology of Guangdong Province & the Key Laboratory of New Energy Technology of Guangdong Universities, School of Chemistry and Chemical Engineering, South China University of Technology, Guangzhou, Guangdong 510641, China.

Longhai Zhang - The Key Laboratory of Fuel Cell Technology of Guangdong Province & the Key Laboratory of New Energy Technology of Guangdong Universities, School of Chemistry and Chemical Engineering, South China University of Technology, Guangzhou, Guangdong

510641, China.

Xiaoxuan Yang - Department of Chemical and Biological Engineering, University at Buffalo, The State University of New York, Buffalo, New York 14260, USA.

Yachao Zeng - Department of Chemical and Biological Engineering, University at Buffalo, The State University of New York, Buffalo, New York 14260, USA.

Yijie Deng - Hunan Province Engineering Technology Research Center of Uranium Tailings

Treatment Technology, School of Resource Environment and Safety Engineering, University

of South China, Hengyang 421001, China.

Mingrui Liu - The Key Laboratory of Fuel Cell Technology of Guangdong Province & the Key Laboratory of New Energy Technology of Guangdong Universities, School of Chemistry and Chemical Engineering, South China University of Technology, Guangzhou, Guangdong 510641, China.

Junlang Huo - The Key Laboratory of Fuel Cell Technology of Guangdong Province & the Key Laboratory of New Energy Technology of Guangdong Universities, School of Chemistry and Chemical Engineering, South China University of Technology, Guangzhou, Guangdong 510641, China.

Chaozhong Li - The Key Laboratory of Fuel Cell Technology of Guangdong Province & the Key Laboratory of New Energy Technology of Guangdong Universities, School of Chemistry and Chemical Engineering, South China University of Technology, Guangzhou, Guangdong 510641, China.

Xiaorong Zhang - The Key Laboratory of Fuel Cell Technology of Guangdong Province & the

Key Laboratory of New Energy Technology of Guangdong Universities, School of Chemistry and Chemical Engineering, South China University of Technology, Guangzhou, Guangdong 510641, China.

Xiudong Shi - The Key Laboratory of Fuel Cell Technology of Guangdong Province & the Key Laboratory of New Energy Technology of Guangdong Universities, School of Chemistry and Chemical Engineering, South China University of Technology, Guangzhou, Guangdong 510641, China.

Yijia Shao - The Key Laboratory of Fuel Cell Technology of Guangdong Province & the Key Laboratory of New Energy Technology of Guangdong Universities, School of Chemistry and Chemical Engineering, South China University of Technology, Guangzhou, Guangdong 510641, China.

Lin Gu - Beijing National Laboratory for Condensed Matter Physics, Institute of Physics, Chinese Academy of Sciences, Beijing 100190, China.

Lirong Zheng - Institute of High Energy Physics, Chinese Academy of Sciences, Beijing 100190, China.

Zhiming Cui - The Key Laboratory of Fuel Cell Technology of Guangdong Province & the Key Laboratory of New Energy Technology of Guangdong Universities, School of Chemistry and Chemical Engineering, South China University of Technology, Guangzhou, Guangdong 510641, China.

Author Contributions

[#]Bin Chi and Longhai Zhang contributed equally to this work.

Notes

The authors declare no competing financial interest.

ACKNOWLEDGEMENTS

The work was supported by the National Natural Science Foundation of China (NSFC Project Nos. 51971094, 21476088, 21776104, 21905045), the Guangdong Provincial Department of Science and Technology (Project No. 2015A030312007), and GuangDong Basic and Applied Basic Research Foundation (2022A1515110126). G.W. thanks the support from the National Science Foundation (CBET-2223467) and the university at buffalo, SUNY.

REFERENCES

- (1) Wang, X. X.; Swihart, M. T.; Wu, G. Achievements, Challenges and Perspectives on Cathode Catalysts in Proton Exchange Membrane Fuel Cells for Transportation. *Nat. Catal.* **2019**, *2* (7), 578-589.
- (2) Deng, Y.; Luo, J.; Chi, B.; Tang, H.; Li, J.; Qiao, X.; Shen, Y.; Yang, Y.; Jia, C.; Rao, P. Advanced Atomically Dispersed Metal–Nitrogen–Carbon Catalysts toward Cathodic Oxygen Reduction in Pem Fuel Cells. *Adv. Energy Mater.* **2021**, *11* (37), 2101222.
- (3) Chen, Y.; Ji, S.; Chen, C.; Peng, Q.; Wang, D.; Li, Y. Single-Atom Catalysts: Synthetic Strategies and Electrochemical Applications. *Joule* **2018**, *2* (7), 1242-1264.
- (4) Ji, S.; Chen, Y.; Wang, X.; Zhang, Z.; Wang, D.; Li, Y. Chemical Synthesis of Single Atomic Site Catalysts. *Chem. Rev.* **2020**, *120* (21), 11900-11955.
- (5) He, Y.; Wu, G. Pgm-Free Oxygen-Reduction Catalyst Development for Proton-Exchange

- Membrane Fuel Cells: Challenges, Solutions, and Promises. *Acc. Mater. Res.* **2022**, *3* (2), 224-236. (6) Wu, G.; More, K. L.; Johnston, C. M.; Zelenay, P. High-Performance Electrocatalysts for Oxygen Reduction Derived from Polyaniline, Iron, and Cobalt. *Science* **2011**, *332* (6028), 443-447.
- (7) Li, Y.; Liu, X.; Zheng, L.; Shang, J.; Wan, X.; Hu, R.; Guo, X.; Hong, S.; Shui, J. Preparation of Fe–N–C Catalysts with Fenx (X = 1, 3, 4) Active Sites and Comparison of Their Activities for the Oxygen Reduction Reaction and Performances in Proton Exchange Membrane Fuel Cells. *J. Mater. Chem. A* **2019**, *7* (45), 26147-26153.
- (8) He, Y.; Hwang, S.; Cullen, D. A.; Uddin, M. A.; Langhorst, L.; Li, B.; Karakalos, S.; Kropf, A. J.; Wegener, E. C.; Sokolowski, J. Highly Active Atomically Dispersed Con₄ Fuel Cell Cathode Catalysts Derived from Surfactant-Assisted Mofs: Carbon-Shell Confinement Strategy. *Energy Environ. Sci.* **2019**, *12* (1), 250-260.
- (9) Li, J.; Chen, M.; Cullen, D. A.; Hwang, S.; Wang, M.; Li, B.; Liu, K.; Karakalos, S.; Lucero, M.; Zhang, H. Atomically Dispersed Manganese Catalysts for Oxygen Reduction in Proton-Exchange Membrane Fuel Cells. *Nat. Catal.* **2018**, *1* (12), 935-945.
- (10) Chen, M.; Li, X.; Yang, F.; Li, B.; Stracensky, T.; Karakalos, S.; Mukerjee, S.; Jia, Q.; Su, D.; Wang, G.; Wu, G.; Xu, H. Atomically Dispersed Mnn4 Catalysts Via Environmentally Benign Aqueous Synthesis for Oxygen Reduction: Mechanistic Understanding of Activity and Stability Improvements. *ACS Catal.* **2020**, *10* (18), 10523-10534.
- (11) Zhang, H.; Hwang, S.; Wang, M.; Feng, Z.; Karakalos, S.; Luo, L.; Qiao, Z.; Xie, X.; Wang, C.; Su, D.; Shao, Y.; Wu, G. Single Atomic Iron Catalysts for Oxygen Reduction in Acidic Media:

- Particle Size Control and Thermal Activation. *Journal of the American Chemical Society* **2017**, 139 (40), 14143-14149.
- (12) Guo, L.; Hwang, S.; Li, B.; Yang, F.; Wang, M.; Chen, M.; Yang, X.; Karakalos, S. G.; Cullen, D. A.; Feng, Z.; Wang, G.; Wu, G.; Xu, H. Promoting Atomically Dispersed Mnn4 Sites Via Sulfur Doping for Oxygen Reduction: Unveiling Intrinsic Activity and Degradation in Fuel Cells. *ACS Nano* **2021**, *15* (4), 6886-6899.
- (13) Zhang, H.; Chung, H. T.; Cullen, D. A.; Wagner, S.; Kramm, U. I.; More, K. L.; Zelenay, P.; Wu, G. High-Performance Fuel Cell Cathodes Exclusively Containing Atomically Dispersed Iron Active Sites. *Energy Environ. Sci.* **2019**, *12* (8), 2548-2558.
- (14) Deng, Y.; Chi, B.; Li, J.; Wang, G.; Zheng, L.; Shi, X.; Cui, Z.; Du, L.; Liao, S.; Zang, K.; Luo, J.; Hu, Y.; Sun, X. Atomic Fe-Doped Mof-Derived Carbon Polyhedrons with High Active-Center Density and Ultra-High Performance toward Pem Fuel Cells. *Adv. Energy Mater.* **2019**, *9* (13), 1802856.
- (15) Wan, X.; Liu, X.; Li, Y.; Yu, R.; Zheng, L.; Yan, W.; Wang, H.; Xu, M.; Shui, J. Fe–N–C Electrocatalyst with Dense Active Sites and Efficient Mass Transport for High-Performance Proton Exchange Membrane Fuel Cells. *Nat. Catal.* **2019**, *2* (3), 259-268.
- (16) Liu, S.; Li, C.; Zachman, M. J.; Zeng, Y.; Yu, H.; Li, B.; Wang, M.; Braaten, J.; Liu, J.; Meyer, H. M.; Lucero, M.; Kropf, A. J.; Alp, E. E.; Gong, Q.; Shi, Q.; Feng, Z.; Xu, H.; Wang, G.; Myers, D. J.; Xie, J.; Cullen, D. A.; Litster, S.; Wu, G. Atomically Dispersed Iron Sites with a Nitrogen–Carbon Coating as Highly Active and Durable Oxygen Reduction Catalysts for Fuel Cells. *Nat. Energy* **2022**, *7* (7), 652-663.

- (17) Kramm, U. I.; Lefevre, M.; Bogdanoff, P.; Schmeisser, D.; Dodelet, J. P. Analyzing Structural Changes of Fe-N-C Cathode Catalysts in Pem Fuel Cell by Mossbauer Spectroscopy of Complete Membrane Electrode Assemblies. *J. Phys. Chem. Lett.* **2014**, *5* (21), 3750-3756.
- (18) Choi, C. H.; Baldizzone, C.; Grote, J. P.; Schuppert, A. K.; Jaouen, F.; Mayrhofer, K. J. Stability of Fe-N-C Catalysts in Acidic Medium Studied by Operando Spectroscopy. *Angew. Chem. Int. Ed.* **2015**, *54* (43), 12753-12757.
- (19) He, Y.; Guo, H.; Hwang, S.; Yang, X.; He, Z.; Braaten, J.; Karakalos, S.; Shan, W.; Wang, M.; Zhou, H.; Feng, Z.; More, K. L.; Wang, G.; Su, D.; Cullen, D. A.; Fei, L.; Litster, S.; Wu, G. Single Cobalt Sites Dispersed in Hierarchically Porous Nanofiber Networks for Durable and High-Power Pgm-Free Cathodes in Fuel Cells. *Adv. Mater.* **2020**, e2003577.
- (20) Baker, Andrew M.; Williams, S. T. D.; Mukundan, R.; Spernjak, D.; Advani, S. G.; Prasad, A. K.; Borup, R. L. Zr-Doped Ceria Additives for Enhanced Pem Fuel Cell Durability and Radical Scavenger Stability. *J. Mater. Chem. A* **2017**, *5* (29), 15073-15079.
- (21) Weissbach, T.; Peckham, T. J.; Holdcroft, S. Ceo 2, Zro 2 and Ysz as Mitigating Additives against Degradation of Proton Exchange Membranes by Free Radicals. *J. Membrane Sci.* **2016**, 498, 94-104.
- (22) Xiao, M.; Chen, Y.; Zhu, J.; Zhang, H.; Zhao, X.; Gao, L.; Wang, X.; Zhao, J.; Ge, J.; Jiang, Z.; Chen, S.; Liu, C.; Xing, W. Climbing the Apex of the Orr Volcano Plot Via Binuclear Site Construction: Electronic and Geometric Engineering. *J. Am. Chem. Soc.* **2019**, *141* (44), 17763-17770.
- (23) Hu, R.; Li, Y.; Zeng, Q.; Shang, J. Role of Active Sites in N-Coordinated Fe-Co Dual-Metal

- Doped Graphene for Oxygen Reduction and Evolution Reactions: A Theoretical Insight. *Appl. Surf. Sci.* **2020**, *525*, 146588.
- (24) Yang, X.; Wang, M.; Zachman, M. J.; Zhou, H.; He, Y.; Liu, S.; Zang, H.-Y.; Feng, Z.; Wu, G. Binary Atomically Dispersed Metal-Site Catalysts with Core—Shell Nanostructures for O2 and Co2 Reduction Reactions. *Small Sci.* **2021**, *1* (10), 2100046.
- (25) He, Y.; Yang, X.; Li, Y.; Liu, L.; Guo, S.; Shu, C.; Liu, F.; Liu, Y.; Tan, Q.; Wu, G. Atomically Dispersed Fe–Co Dual Metal Sites as Bifunctional Oxygen Electrocatalysts for Rechargeable and Flexible Zn–Air Batteries. *ACS Catal.* **2022**, *12* (2), 1216-1227.
- (26) Zhou, Y.; Yang, W.; Utetiwabo, W.; Lian, Y. M.; Yin, X.; Zhou, L.; Yu, P.; Chen, R.; Sun, S. Revealing of Active Sites and Catalytic Mechanism in N-Coordinated Fe, Ni Dual-Doped Carbon with Superior Acidic Oxygen Reduction Than Single-Atom Catalyst. *J. Phys. Chem. Lett.* **2020**, *11* (4), 1404-1410.
- (27) Li, Y.; Shan, W.; Zachman, M. J.; Wang, M.; Hwang, S.; Tabassum, H.; Yang, J.; Yang, X.; Karakalos, S.; Feng, Z.; Wang, G.; Wu, G. Atomically Dispersed Dual-Metal Site Catalysts for Enhanced Co2 Reduction: Mechanistic Insight into Active Site Structures. *Angew. Chem. Int. Ed.* **2022**, *61* (28), e202205632.
- (28) Tang, H.; Cai, S.; Xie, S.; Wang, Z.; Tong, Y.; Pan, M.; Lu, X. Metal-Organic-Framework-Derived Dual Metal- and Nitrogen-Doped Carbon as Efficient and Robust Oxygen Reduction Reaction Catalysts for Microbial Fuel Cells. *Adv. Sci.* **2016**, *3* (2), 1500265.
- (29) Han, X.; Ling, X.; Yu, D.; Xie, D.; Li, L.; Peng, S.; Zhong, C.; Zhao, N.; Deng, Y.; Hu, W. Atomically Dispersed Binary Co-Ni Sites in Nitrogen-Doped Hollow Carbon Nanocubes for

Reversible Oxygen Reduction and Evolution. Adv. Mater. 2019, 31 (49), e1905622.

- (30) Lu, Z.; Wang, B.; Hu, Y.; Liu, W.; Zhao, Y.; Yang, R.; Li, Z.; Luo, J.; Chi, B.; Jiang, Z.; Li, M.; Mu, S.; Liao, S.; Zhang, J.; Sun, X. An Isolated Zinc-Cobalt Atomic Pair for Highly Active and Durable Oxygen Reduction. *Angew. Chem. Int. Ed.* **2019**, *58* (9), 2622-2626.
- (31) Yang, X.; Priest, C.; Hou, Y.; Wu, G. Atomically Dispersed Dual-Metal-Site Pgm-Free Electrocatalysts for Oxygen Reduction Reaction: Opportunities and Challenges. *SusMat* **2022**.
- (32) Li, J.; Zhang, H.; Samarakoon, W.; Shan, W.; Cullen, D. A.; Karakalos, S.; Chen, M.; Gu, D.; More, K. L.; Wang, G.; Feng, Z.; Wang, Z.; Wu, G. Thermally Driven Structure and Performance Evolution of Atomically Dispersed Fen4 Sites for Oxygen Reduction. *Angew. Chem. Int. Ed.* **2019**, *58* (52), 18971-18980.
- (33) Wang, Y.; Chen, X.; Lin, Q.; Kong, A.; Zhai, Q.-G.; Xie, S.; Feng, P. Nanoporous Carbon Derived from a Functionalized Metal-Organic Framework as a Highly Efficient Oxygen Reduction Electrocatalyst. *Nanoscale* **2017**, *9* (2), 862-868.
- (34) Asset, T.; Atanassov, P. Iron-Nitrogen-Carbon Catalysts for Proton Exchange Membrane Fuel Cells. *Joule* **2020**, *4* (1), 33-44.
- (35) Huang, L.; Chen, J.; Gan, L.; Wang, J.; Dong, S. Single-Atom Nanozymes. *Sci. Adv.* **2019**, *5* (5), eaav5490.
- (36) Pan, Y.; Liu, S.; Sun, K.; Chen, X.; Wang, B.; Wu, K.; Cao, X.; Cheong, W. C.; Shen, R.; Han, A.; Chen, Z.; Zheng, L.; Luo, J.; Lin, Y.; Liu, Y.; Wang, D.; Peng, Q.; Zhang, Q.; Chen, C.; Li, Y. A Bimetallic Zn/Fe Polyphthalocyanine-Derived Single-Atom Fe-N4 Catalytic Site: A Superior Trifunctional Catalyst for Overall Water Splitting and Zn-Air Batteries. *Angew. Chem. Int. Ed.*

- **2018**, *57* (28), 8614-8618.
- (37) Qiao, M.; Wang, Y.; Wang, Q.; Hu, G.; Mamat, X.; Zhang, S.; Wang, S. Hierarchically Ordered Porous Carbon with Atomically Dispersed Fen4 for Ultraefficient Oxygen Reduction Reaction in Proton-Exchange Membrane Fuel Cells. *Angew. Chem. Int. Ed.* **2020**, *59* (7), 2688-2694.
- (38) Jiao, L.; Zhang, R.; Wan, G.; Yang, W.; Wan, X.; Zhou, H.; Shui, J.; Yu, S. H.; Jiang, H. L. Nanocasting Sio2 into Metal-Organic Frameworks Imparts Dual Protection to High-Loading Fe Single-Atom Electrocatalysts. *Nat. Commun.* **2020**, *11* (1), 2831.
- (39) Lai, Q.; Zheng, L.; Liang, Y.; He, J.; Zhao, J.; Chen, J. Metal-Organic-Framework-Derived Fe-N/C Electrocatalyst with Five-Coordinated Fe-Nx Sites for Advanced Oxygen Reduction in Acid Media. *ACS Catal.* **2017**, *7* (3), 1655-1663.
- (40) Zhang, Y.; Liu, J.; Wang, J.; Zhao, Y.; Luo, D.; Yu, A.; Wang, X.; Chen, Z. Engineering Oversaturated Fe-N5 Multifunctional Catalytic Sites for Durable Lithium-Sulfur Batteries. *Angew. Chem. Int. Ed.* **2021**.
- (41) Huang, J.; Lu, Q.; Ma, X.; Yang, X. Bio-Inspired Fen₅ Moieties Anchored on a Three-Dimensional Graphene Aerogel to Improve Oxygen Reduction Catalytic Performance. *J. Mater. Chem. A* **2018**, *6* (38), 18488-18497.
- (42) Zhao, Y. M.; Zhang, P. C.; Xu, C.; Zhou, X. Y.; Liao, L. M.; Wei, P. J.; Liu, E.; Chen, H.; He, Q.; Liu, J. G. Design and Preparation of Fe-N5 Catalytic Sites in Single-Atom Catalysts for Enhancing the Oxygen Reduction Reaction in Fuel Cells. *ACS Appl. Mater. Interfaces* **2020**, *12* (15), 17334-17342.
- (43) Luo, X.; Wei, X.; Wang, H.; Gu, W.; Kaneko, T.; Yoshida, Y.; Zhao, X.; Zhu, C. Secondary-

- Atom-Doping Enables Robust Fe-N-C Single-Atom Catalysts with Enhanced Oxygen Reduction Reaction. *Nano-Micro Lett.* **2020**, *12* (1).
- (44) Sun, H.; Wang, M.; Du, X.; Jiao, Y.; Liu, S.; Qian, T.; Yan, Y.; Liu, C.; Liao, M.; Zhang, Q.; Meng, L.; Gu, L.; Xiong, J.; Yan, C. Modulating the D-Band Center of Boron Doped Single-Atom Sites to Boost the Oxygen Reduction Reaction. *J. Mater. Chem. A* **2019**, *7* (36), 20952-20957.
- (45) Malko, D.; Kucernak, A.; Lopes, T. In Situ Electrochemical Quantification of Active Sites in Fe-N/C Non-Precious Metal Catalysts. *Nat. Commun.* **2016**, *7*, 13285.
- (46) Jeon, M. K.; Won, J. Y.; Oh, K. S.; Lee, K. R.; Woo, S. I. Performance Degradation Study of a Direct Methanol Fuel Cell by Electrochemical Impedance Spectroscopy. *Electrochim. Acta* **2007**, *53* (2), 447-452.
- (47) Yang, X.; Zeng, Y.; Alnoush, W.; Hou, Y.; Higgins, D.; Wu, G. Tuning Two-Electron Oxygen-Reduction Pathways for H2o2 Electrosynthesis Via Engineering Atomically Dispersed Single Metal Site Catalysts. *Adv. Mater.* **2022**, *34* (23), 2107954.
- (48) Pan, F.; Yang, X.; O'Carroll, T.; Li, H.; Chen, K.-J.; Wu, G. Carbon Catalysts for Electrochemical Co2 Reduction toward Multicarbon Products. *Adv. Energy Mater.* **2022**, *12* (24), 2200586.
- (49) Yang, X.; Mukherjee, S.; O'Carroll, T.; Hou, Y.; Singh, M. R.; Gauthier, J. A.; Wu, G. Achievements, Challenges, and Perspectives on Nitrogen Electrochemistry for Carbon-Neutral Energy Technologies. *Angew. Chem. Int. Ed.* **2023**, *62* (10), e202215938.
- (50) Zhu, H.; Ren, X.; Yang, X.; Liang, X.; Liu, A.; Wu, G. Fe-Based Catalysts for Nitrogen Reduction toward Ammonia Electrosynthesis under Ambient Conditions. *SusMat* **2022**, *2* (3), 214-

242.